Schweizerischer Erdbebendienst
Service Sismologique Suisse
Servizio Sismico Svizzero
Swiss Seismological Service

ETH zürich

SITE CHARACTERIZATION REPORT

SCOD: Château d'Oex (VD) - Salle de spectacle

Clotaire Michel, Marco Pilz, Manuel Hobiger, Donat Fäh

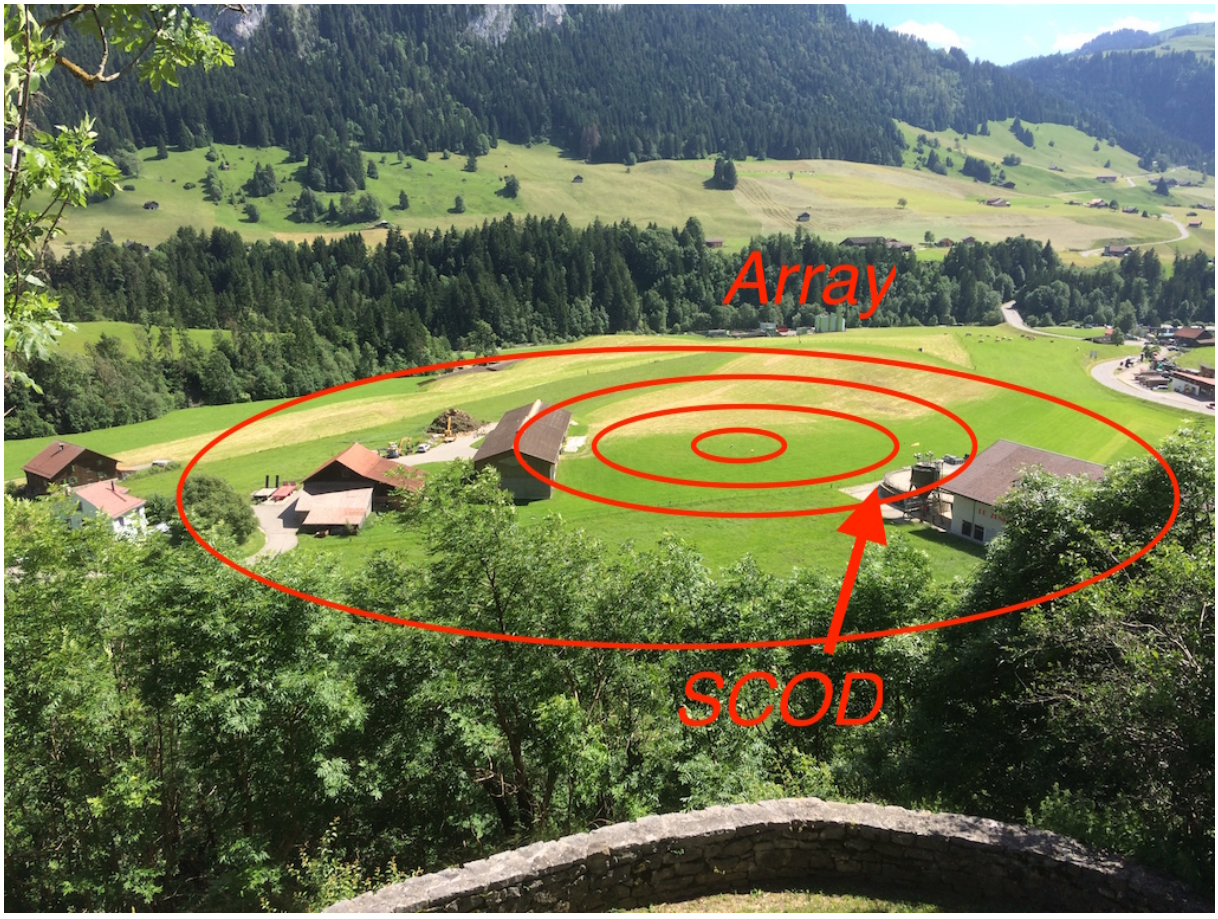

Last Modification: 12th October, 2016

Schweizerischer Erdbebendienst (SED)
Service Sismologique Suisse
Servizio Sismico Svizzero
Servizi da Terratrembels Svizzer

ETH Zurich
Sonneggstrasse 5
8092 Zurich
Schweiz
clotaire@sed.ethz.ch

Contents

Summary

The new station SCOD was installed in the town of Château d'Oex (VD) and the installation site has been characterized. We performed passive seismic array measurements that successfully allowed to retrieve 1D velocity profile at the station site. The sedimentary cover (alluvial fan) is about 5 m thickness with a velocity of 270 m/s. The rock below (Upper Cretaceous marly limestone) has a velocity of about 1400 m/s. The thickness of the cover and the rock characteristics are very variable below the town.
$V_{s,30}$ is 860 m/s and the site corresponds to ground type E in the Eurocode 8 (CEN, 2004) and SIA261 (SIA, 2014). The theoretical 1D SH transfer function computed from the inverted profiles shows deamplification at low frequency and a strong amplification at the resonance frequency of the cover around 13 Hz.

1 Introduction

In the framework of the second phase of the Swiss Strong Motion Network (SSMNet) renewal project, a new installation in Château d'Oex (VD), in the field hosting the International Balloon Festival was decided. It is located in the Sarine valley (see Fig. 1), in a mountain area with shallow layers of moraine and alluvial fan. The new station went operational on 20 April 2016.

Figure 1: Station SCOD (in front of the access ramp) and town of Château d'Oex in the background, taken form the top of the morainic hill. The church is located on a rock outcrop.

2 Geological setting

The site is located in the valley of the Sarine river in a mountain area. The loose deposits are mostly related to alluvial fans, rock slope debris and moraine. According to the geological data of Swisstopo (see Fig. 4), the site SCOD is located on an alluvial fan as most of the town, with the noticeable exception of the church (Fig. 1). The hill in the South of site SCOD where part of the geophysical measurement was performed is made of moraine. According to the geological map, the bedrock below the town is changing following SW-NE bands: In the North, it is made of flysch (sandstone and schist with conglomerates) of Upper Cretaceous from the Simme nappe. The second band, including the church site is made of marly limestones and calc-schists of Eocene age (Tertiary) on top of marly limestones of upper Cretaceous age from the median fore-alpine nappe. The third band where the station and the array are located, is split in two parts (N and S) and is made of this last Upper Cretaceous marly limestone according to the geological map. The thickness of the unconsolidated layers is most probably very variable.
This site is classified as ground type E (SIA261) by the Federal Office for the Environment.

3 Site characterization using passive measurements

3.1 Measurements and data set

We investigated the local underground structure by passive seismic array measurements which took place on June 28th, 2016. The layout of the seismic arrays is shown in Fig. 2. Two configurations were used.
The parameters of both arrays are given in Table 1. For these measurements 12 Nanometrics Centaur dataloggers named NR42 to NR49 and NR52 to NR55 and 14 Lennartz 3C 5 s seismometers were available. Each datalogger can record on 2 ports A (channels EH1, EH2, EH3 for Z, N, E directions) and B (channels EH4, EH5, EH6 for Z, N, E directions). Time synchronization is ensured by GPS. The sensors were placed on a metal tripod, in a 20 cm deep hole, when possible, for better coupling with the ground.
The sensor coordinates were measured using a differential GPS device (Leica Viva GS10), including only a rover station and using the Real Time Kinematic technique provided by Swisstopo. It allows an absolute positioning with an accuracy better than 4 cm on the Swissgrid.

Table 1: List of the seismic array measurements in Château d'Oex.

Array name	Number of sensors	Minimum interstation distance [m]	Aperture [m]	Recording time [min]
COD1	14	10	120	125
COD2	14	10	235	123

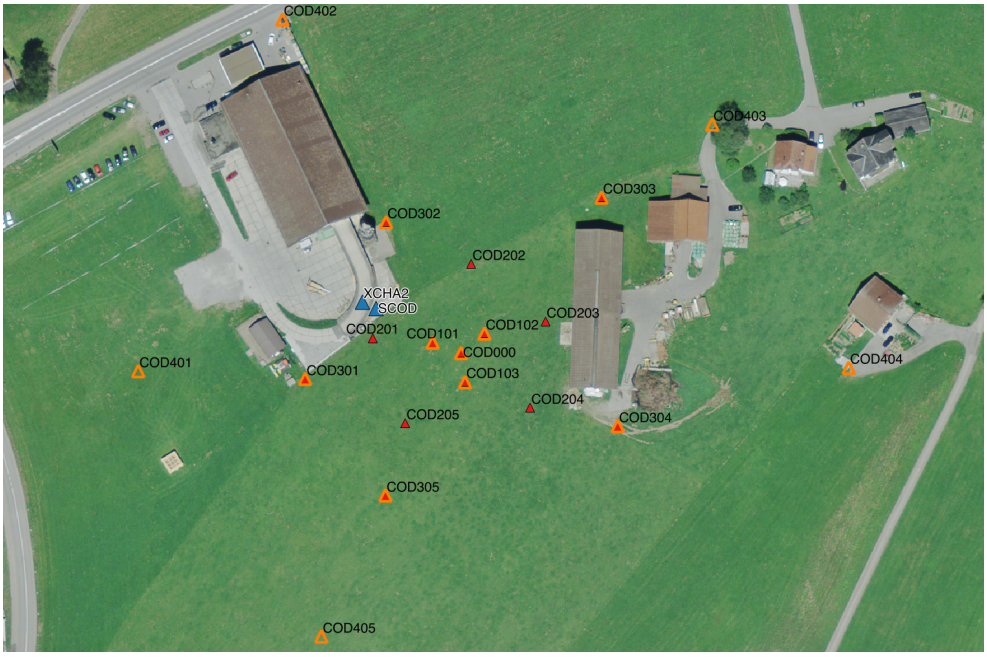

Figure 2: Layout of the array measurements at site SCOD.

The largest time windows were extracted, for which all the sensors of the array were correctly placed and the GPS synchronization was ensured. Disturbances, possibly due to wind, can be noticed at low frequency. Large peaks due to anthropogenic disturbances are locally noticed above 10 Hz. Their origin is unclear but could be related to electric fences. The most noticeable can be found at point COD101 at 28 Hz. Point COD201 shows a strange spectrum that may be due to a cable problem and this recording should not be used. Point COD302 also shows an unexpected signal at 2.1 Hz that is most probably due to the resonance of the silo located nearby. Moreover, it shows the lower noise level that could be explained by the fact that it was protected from the wind. Point COD402, located along the main road at the gas station shows an elevated level of disturbances in the vertical component and an unexpected peak at 2.5 Hz in the E component.
Orientations of the sensors could not be checked by maximizing the correlation with the central station at low frequencies (Poggi et al., 2012b).

3.2 Single station measurements results

3.2.1 H/V curves

The H/V curves show a similar shape across the array below 4 Hz (Fig. 3). A bump can be observed at 0.65 Hz that is not interpreted as related to the geology since it is not present in previous measurements in Château d'Oex, especially at the temporary station XCHA2, located in a technical room below the ramp close to SCOD (Fig. 2), that recorded during several days (see Fig. 6). Therefore, this bump is maybe related to wind. More generally, the high values of the H/V ratios during the measurement can be related to wind and the H/V ratios cannot be used as proxy for the Rayleigh wave ellipticity.
Another peak is observed at most of the stations with a large variability between 6.9 and 20 Hz. It is not always clearly defined and therefore subjected to a large uncertainty. It is particularly clear close to SCOD with a frequency of 10 to 13 Hz. Unfortunately, station COD201 that was the closest to the station did not work properly as explained above. Fig. 4 shows the distribution of the values of this peak, together with the results of a single station array campaign performed previously in the town: values around 10 Hz are found between the main road and the foot of the hill. On the hillside, the value increase to about 15 Hz and are absent at the hilltop. They decrease slightly on the other side of the hill (COD404). According to the geological map, the hill is made of moraine, surrounded by alluvial fans. The resonance peaks can therefore be interpreted as representing the resonance of a layer of less than 15 m of unconsolidated sediments of alluvial origin that can be found in the depressions and with lower thicknesses on the hillsides.

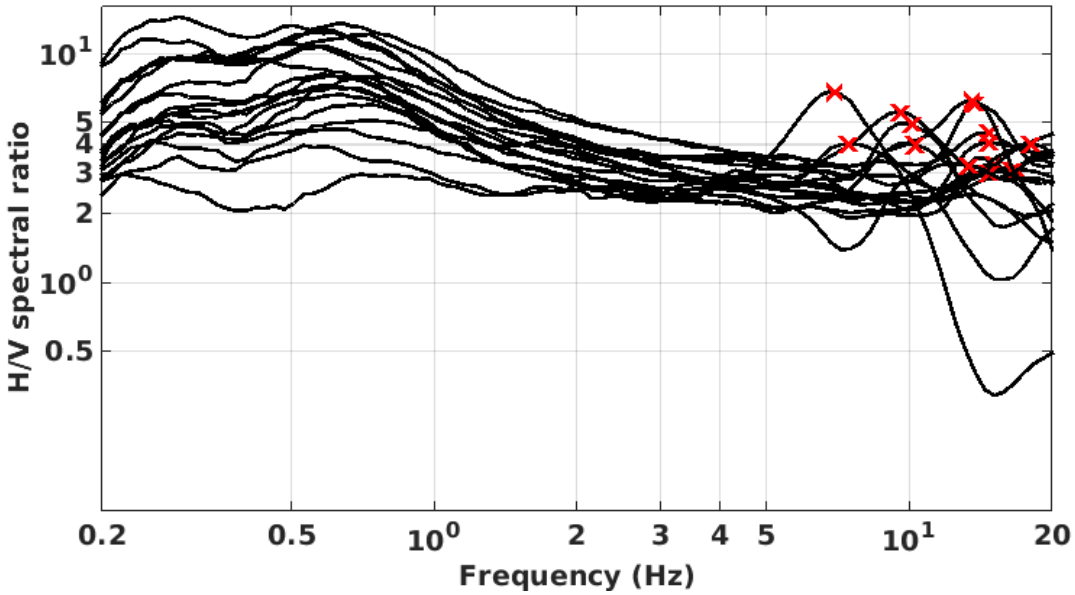

Figure 3: Comparison of H/V spectral ratios (time-frequency analysis code V. Poggi) between the different points of the arrays. The curve reaching values below 1 corresponds to point COD402 located at the petrol station and should not be interpreted.

Moreover, all the methods to compute H/V ratios are compared at point COD301 in Fig. 5, in which the classical methods were divided by $\sqrt{2}$ to correct from the Love

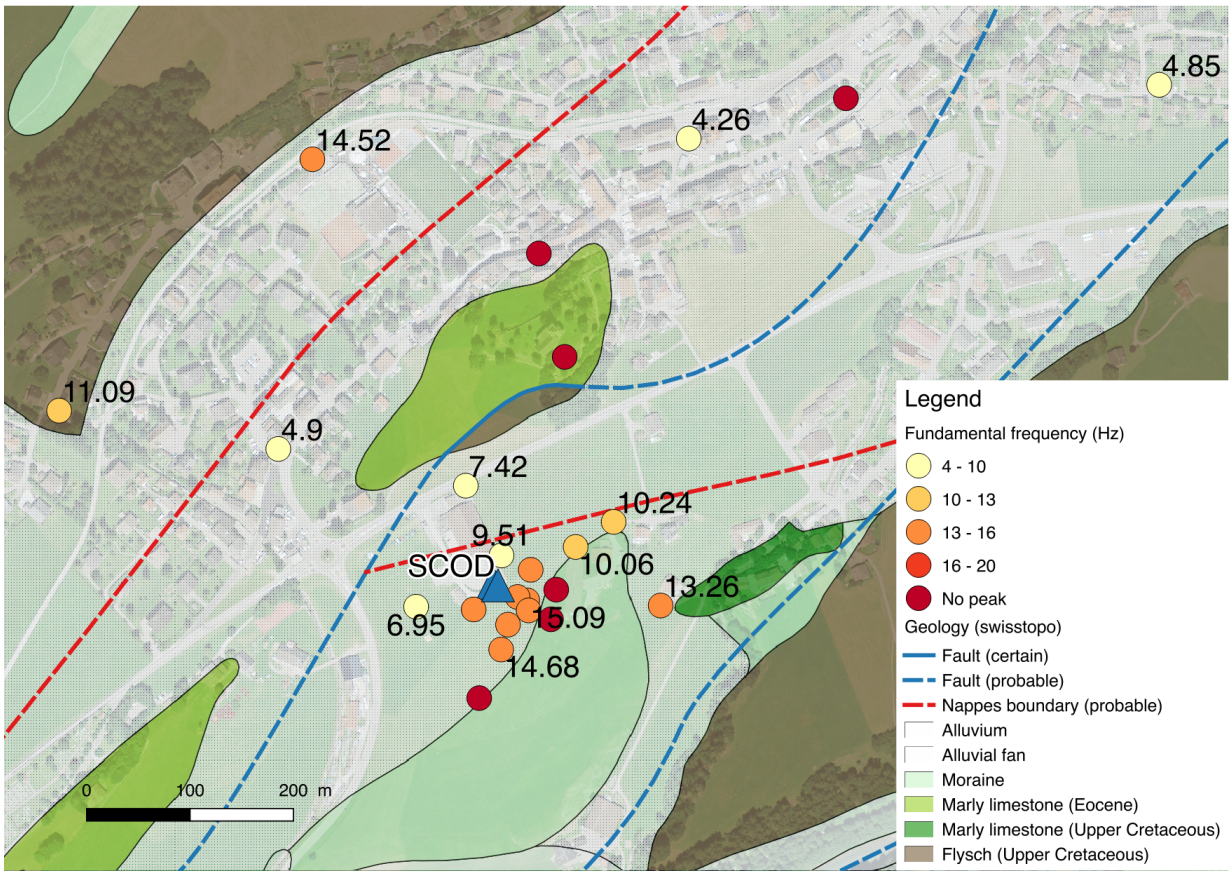

Figure 4: Maps of the identified peaks in the H/V ratios superimposed on the simplified geological map of the area.

wave contribution (Fäh et al., 2001). The classical and TFA methods do not match at low frequency, showing that this correction was not useful. Again, this part is anyway affected by disturbances, possibly wind. The 3C FK analysis (Capon method) matches with the H/V analysis with a slightly shifted peak and lower amplitudes at the peak.
The H/V ratios of temporary station XCHA2 and permanent SCOD are compared in Fig. 6. The data from accelerometric station SCOD is only instrumental noise below 5 Hz, but station XCHA2 shows that the H/V ratios are flat (value about 1) below this frequency. Both show a peak at high frequency but shifted (10 Hz at XCHA2 and 13 Hz at SCOD) since the stations themselves were slightly shifted. Note that the high peak in the H/V ratios of SCOD is related to an anthropogenic disturbance, the true peak is located at slightly higher frequency.
The fundamental peak at the SCOD station is therefore at 13 Hz, with a peak amplitude around 3.5.

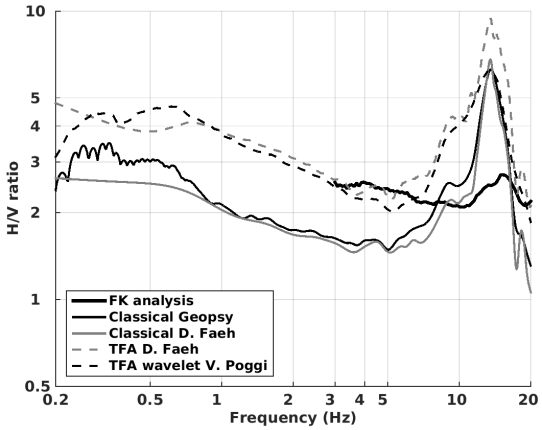

Figure 5: H/V spectral ratios for point COD301 using the different codes. Classical methods were divided by $\sqrt{2}$.

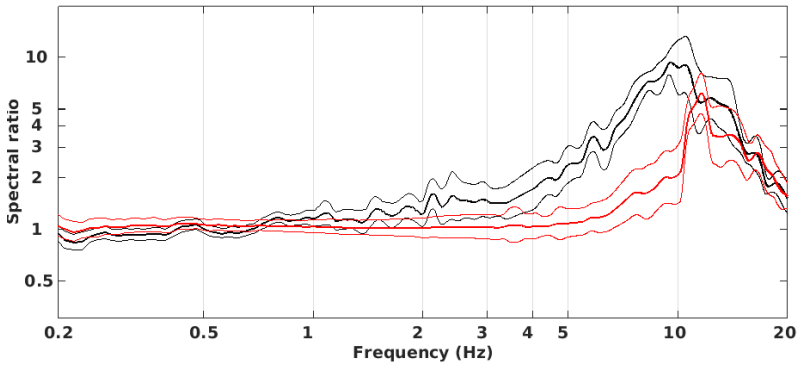

Figure 6: Comparison of H/V ratios of temporary station XCHA2 (black lines, mean and one standard deviation) and station SCOD (red lines, mean and one standard deviation). While XCHA2 station is made of a broadband seismometer, SCOD station is made of an accelerometer and displays only electronic noise below 5 Hz.

3.2.2 Polarization analysis

Polarization analysis on the array data was performed to check for 2D resonance using the method of Burjánek et al. (2010). All points (Fig. 7) show a relatively flat motion at low frequency corresponding to the 0.65 Hz peak in the H/V ratios with a diffuse polarization that may be related to wind. The peak corresponding to the unconsolidated sediments is relatively polarized but the directions are not consistent within the array. We assume therefore that there is no 2D behaviour of the valley at this site.

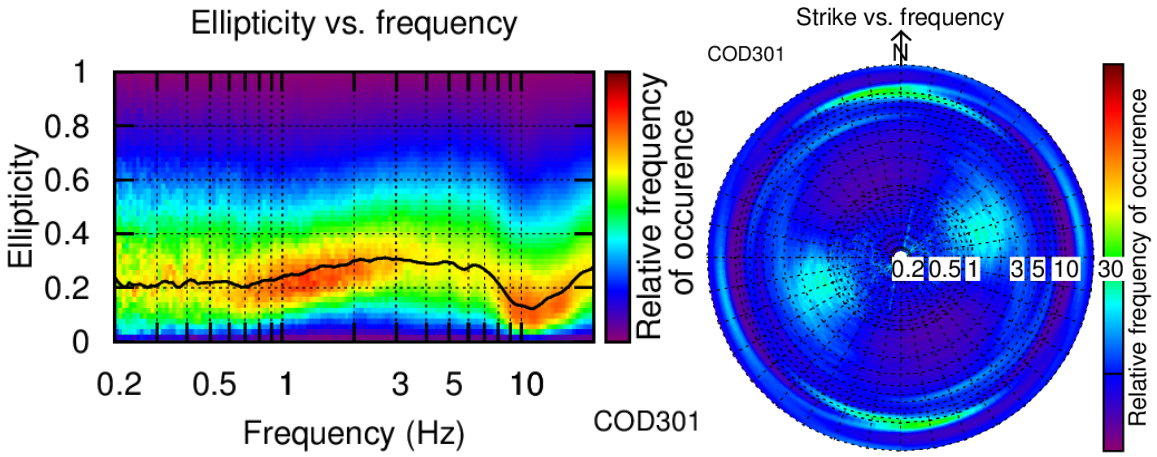

Figure 7: Polarization analysis at point COD301. Left: Ellipticity (A trough in the ellipticity corresponds to polarized motion). Right: Strike of the polarization.

3.3 Array analysis results

The results of the 3-component high-resolution FK analysis (Poggi and Fäh, 2010) for the merged results of both configurations are shown in Fig. 8. The fundamental mode of Love waves is clearly determined from this analysis between 6 and 17 Hz. This is surprising considering the that the upper layers are highly variable. The contribution to the curve above 10 Hz is most probably limited to few stations close to the centre of the array where the resonance is at about 13 Hz (kink in the dispersion curve). This corresponds well to the station site and this picking is therefore used in the following. From the vertical component, some curves difficult to interpret can be retrieved. They could correspond to the fundamental mode of Rayleigh waves, to the fundamental and the first higher mode or to a mix of both (see the interpretation in the following section). The ellipticity curve determined with the 3-component HRFK analysis is comparable to the H/V analysis, with a peak frequency around 15 Hz.

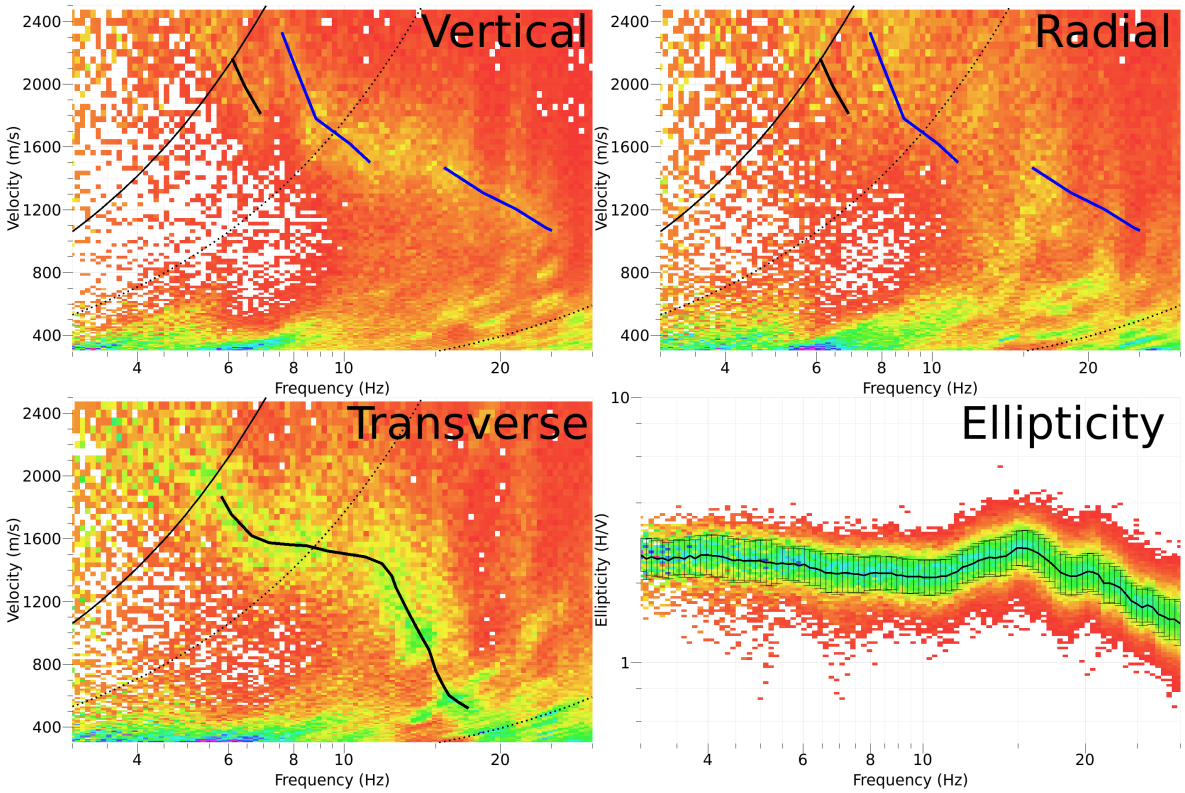

Figure 8: Dispersion curves obtained from the 3C HRFK analyses. Two interpretations are proposed for Rayleigh waves (vertical and radial, see text).

3.4 Interpretation

Fig. 9 gives an overview of the dispersion curves determined from the different datasets. The curves are retrieved between 6 and 17 Hz with velocities ranging from about 1800 m/s at 6 Hz down to 500 m/s at 17 Hz for the fundamental Love mode. In the following, two interpretations of Ralyeigh waves are used: the first one (in black in Fig. 8) corresponds to a small chunk of the fundamental mode of Rayleigh waves and the rest is not interpreted. The second interpretation corresponds to the fundamental and first higher modes of Rayleigh waves (in blue in in Fig. 8).

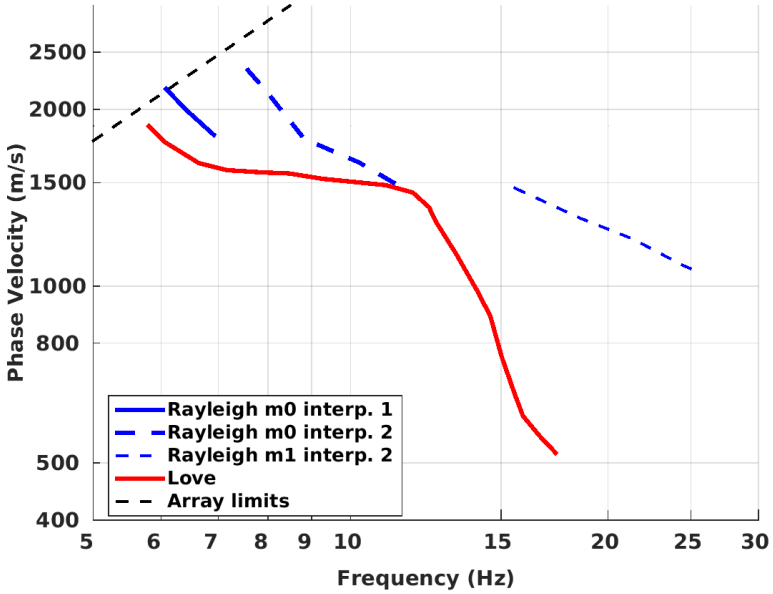

Figure 9: Picked dispersion curves from 3C HRFK analysis.

3.5 Data inversion

The inversion of the surface waves properties into 1D velocity profiles was performed using the Improved Neighborhood Algorithm (NA) (Wathelet, 2008) implemented in the Dinver software.

3.5.1 Misfit function

Although the structure is not 1D for the upper layers, the picked Love dispersion curve is a strong constrain towards a velocity structure with a fundamental frequency around 13 Hz, i.e. at the station site. Both interpretations of Rayleigh wave dispersion curves were used in two different misfit functions. In the first function, the small chunk of Rayleigh fundamental mode dispersion curves, the Love fundamental dispersion curve and the right flank of the ellipticity curve (H/V curve at SCOD station) were used as simultaneous targets without standard deviation. A low weight of 0.1 was assigned to the ellipticity curve. In the second function, the Rayleigh fundamental and first higher modes (second interpretation) and the Love fundamental mode dispersion curves were used. The weight on the Love dispersion curves was set as 50. The ellipticity curve was not used in the inversion. In both cases, all curves were resampled using 50 points between 3 and 30 Hz in log scale.

3.5.2 Parametrization of the model space

The velocity was assumed to increase with depth. A posteriori, we showed that no velocity inversion is needed to explain the observed data. The Poisson ratio was inverted in each layer in the range 0.2-0.4 (no aquifer). The density was assumed to be 2000 kg/m^3 in the first layer and 2500 kg/m^3 in the bedrock. Inversions with free layer depths as well as fixed layer depths were performed. 3 layers are enough to explain most of the targets (dispersion and ellipticity), but more layers are used to smooth the obtained results and better explore the parameter space. 3 independent runs of 5 different parametrization schemes (4 and 5 layers over a half space and 9, 9 and 11 layers with fixed depth) for 2 different misfit functions were performed, i.e. a total of 30 runs.

3.5.3 Results

Examples of retrieved ground profiles for these two strategies are presented in Fig. 10 and Fig. 11. When comparing to the target curves (Fig. 12), dispersion curves are generally well reproduced but no the right flank of the ellipticity. This is expected considering the variability of the thin layer of sediments producing this peak. Moreover, the picking of the Love dispersion curve was highly subjective and this is no surprise that the shape of the retrieved models show a less pronounced kink as the picked curve. For further elaborations, the best models of these 30 runs were selected and used (see section 4.1).

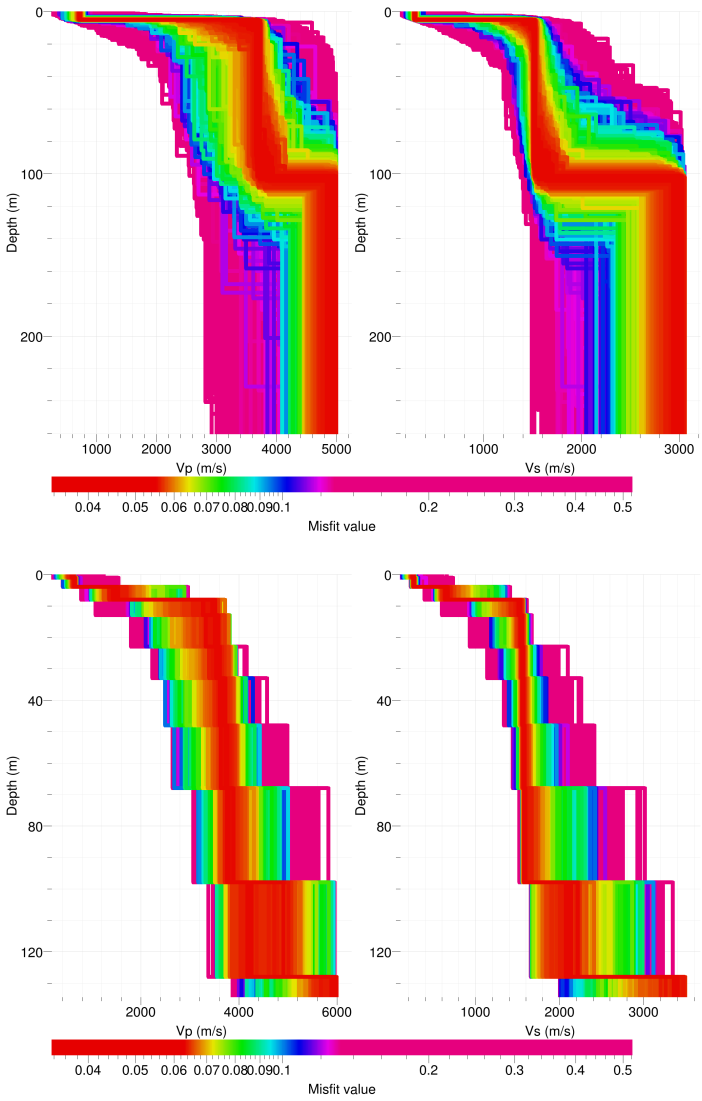

Figure 10: Inverted ground profiles at SCOD in terms of V_p and V_s for the first interpretation of Rayleigh waves; top: free layer depth strategy; bottom: fixed layer depth strategy.

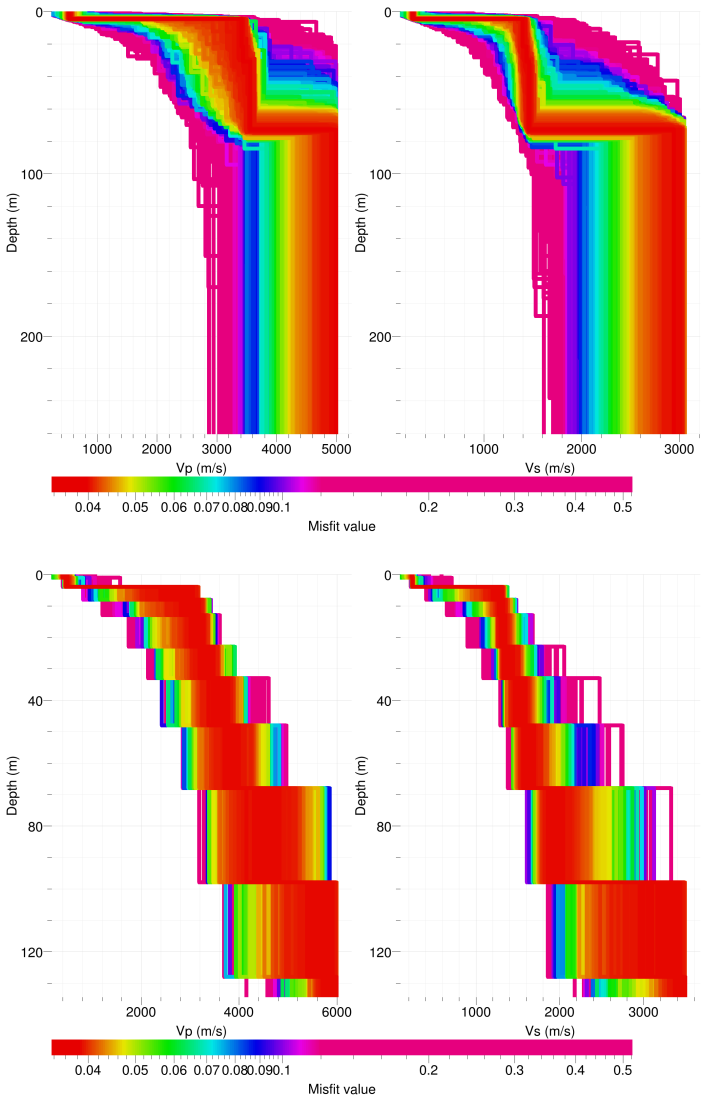

Figure 11: Inverted ground profiles at SCOD in terms of V_p and V_s for the second interpretation of Rayleigh waves; top: free layer depth strategy; bottom: fixed layer depth strategy.

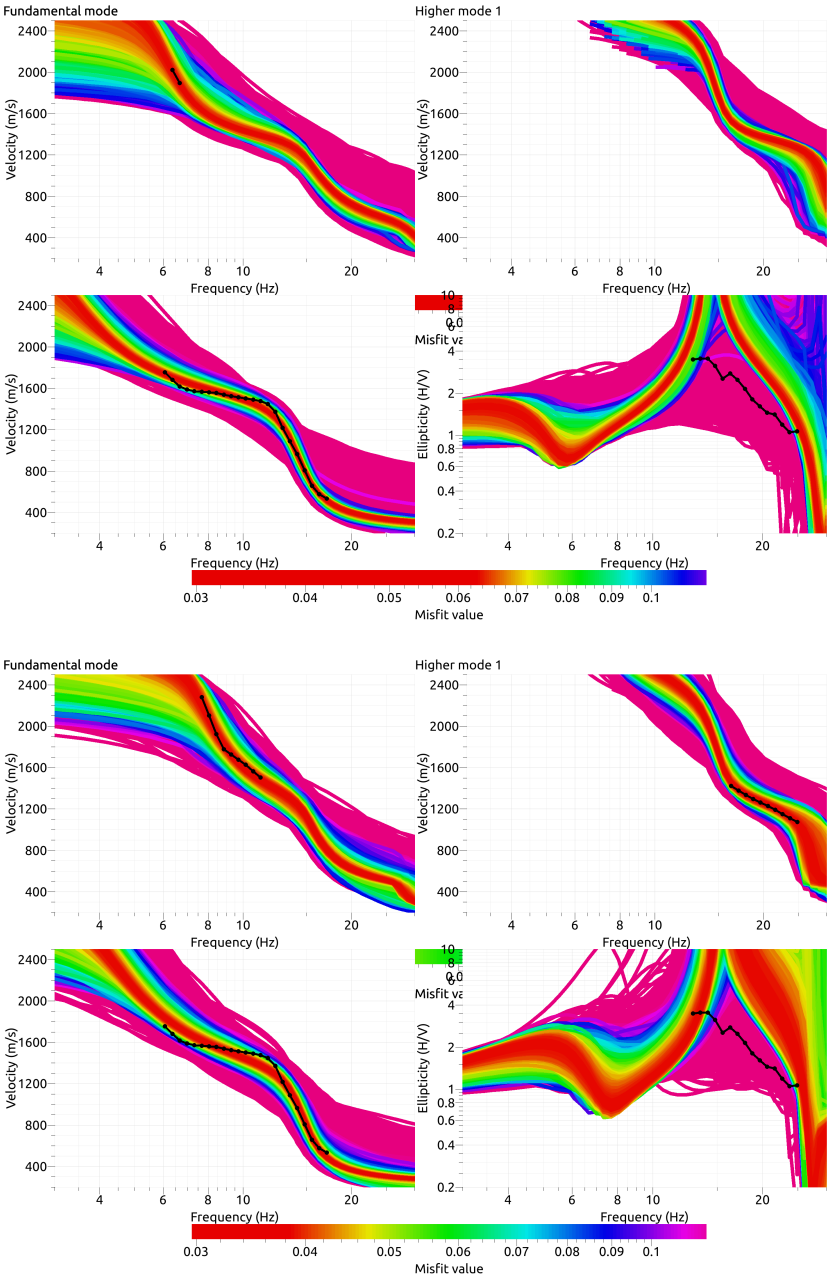

Figure 12: Comparison between inverted models and measured Rayleigh (top row;fundamental mode: left, first higher mode: right) and Love (bottom row left) modes and corresponding ellipticity (bottom row, right) at SCOD site fir the first (top figures) and second (bottom figures) interpretations.

4 Interpretation of the velocity profiles

4.1 Velocity profiles

As already explained, the chosen Love dispersion curve is a strong constrain towards a velocity structure corresponding to the station site so that no variation in the upper structure is retrieved, although the site below the array shows strong lateral variations. The first five meter of the profile are found to have a velocity of 270 m/s and correspond to the alluvial fan cover. The selected dispersion curves constrain well the first interface but not the velocity in the 2 first meters. The velocity contrast is strong with the underlaying rock at about 1400 m/s. Depending on the interpretation of the dispersion curves, the velocity is increasing again below 70 or 100 m depth towards the basement velocity that is poorly constrained.
Assuming this velocity for the alluvial cover, the retrieved H/V peaks in the town indicate a maximum cover of 15 m of sediments (Fig. 4).

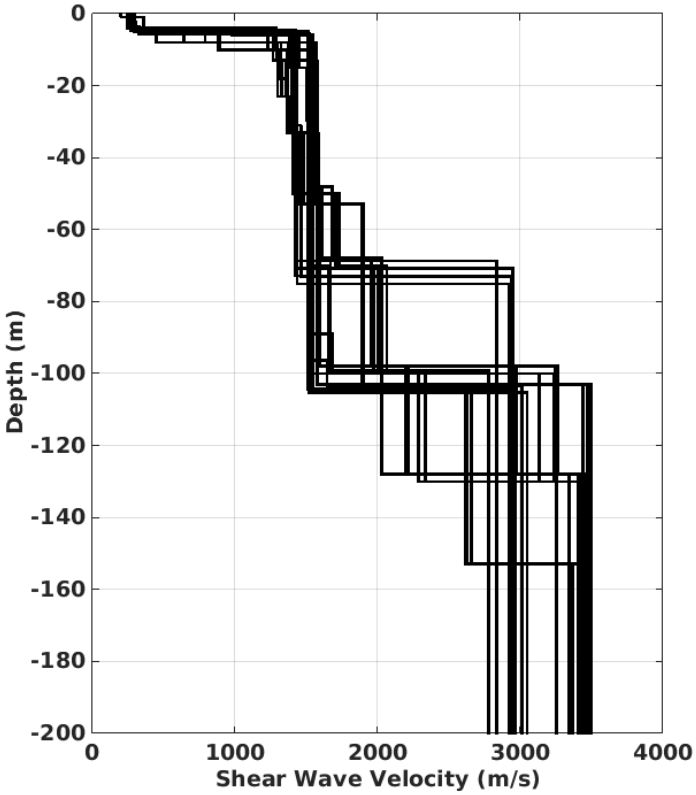

Figure 13: Shear-wave velocity profiles of the 30 selected models.

The distribution of the travel time average velocities at different depths was computed from the selected models. $V_{s,30}$ is found to be 860 m/s, but this site corresponds to class E in the Eurocode 8 (CEN, 2004) and the SIA261 (SIA, 2014).

4.2 Quarter-wavelength representation

The quarter-wavelength velocity approach (Joyner et al., 1981) provides, for a given frequency, the average velocity at a depth corresponding to 1/4 of the wavelength of interest. It is useful to identify the frequency limits of the experimental data (minimum frequency in dispersion curves at 5.8 Hz). The results using this proxy show that the dispersion curves constrain the profiles down to 44 m (Fig. 14). Moreover, the quarter wavelength impedance-contrast introduced by Poggi et al. (2012a) is also displayed in the figure. It corresponds to the ratio between two quarter-wavelength average velocities, respectively from the top and the bottom part of the velocity profile, at a given frequency (Poggi et al., 2012a). It shows a trough (inverse shows a peak) at the resonance frequency.

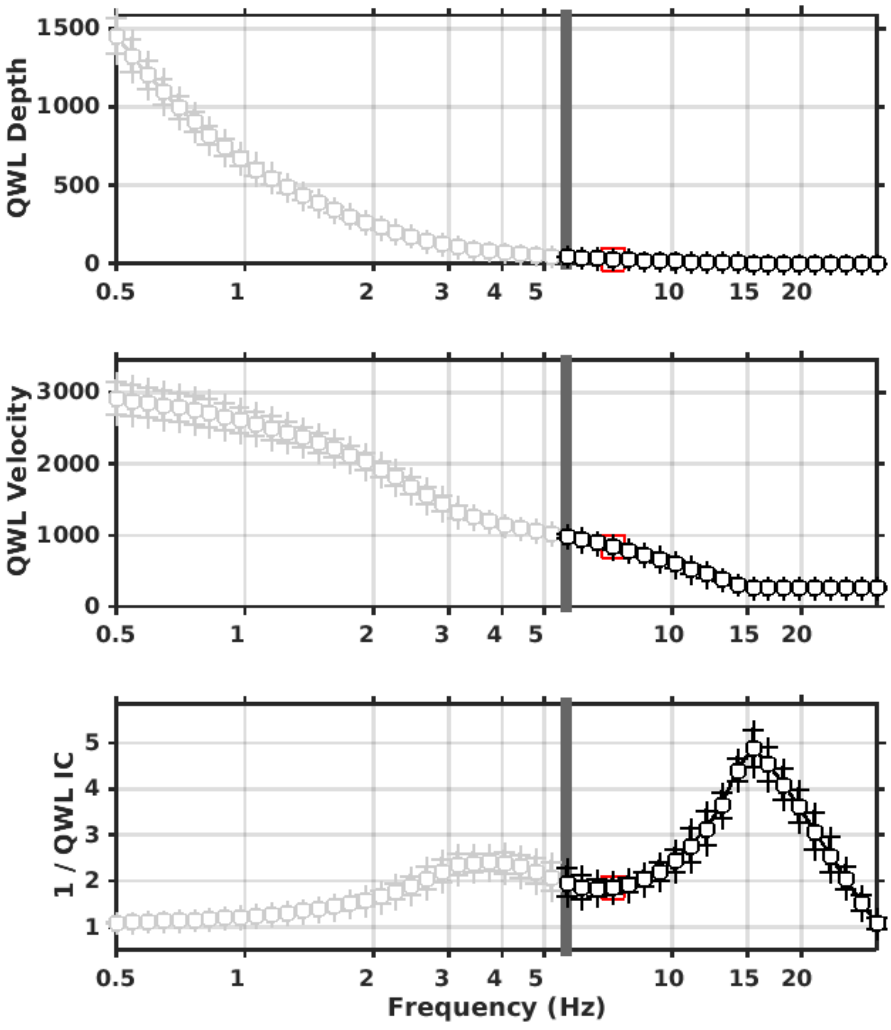

Figure 14: Quarter wavelength representation of the velocity profile for the selected velocity profiles (top: depth, center: velocity, bottom: inverse of the impedance contrast). The black curves are constrained by the dispersion curves, the light grey curves are not constrained by the data. The red square corresponds to V_{S30}.

4.3 SH transfer function

The theoretical SH-wave transfer function for vertical propagation (Roesset, 1970) is computed from the selected profiles. It is corrected with respect to the Swiss Reference Rock model (Poggi et al., 2011) following Edwards et al. (2013). It shows a large peak at the fundamental frequency of resonance reaching an amplification of 6 and de-amplification at low frequencies (Fig. 15).

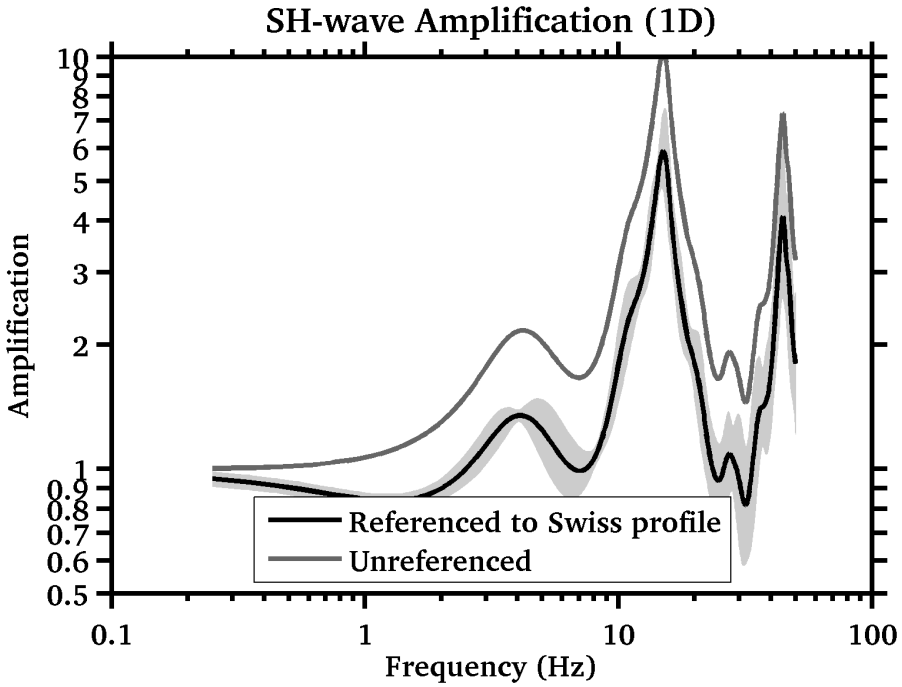

Figure 15: Amplification at site SCOD with respect to the local bedrock and to the Swiss reference rock model with its standard deviation.

5 Conclusions

The passive measurement presented in this study were successful in deriving a velocity model for the site Château d'Oex (SCOD station). The sedimentary cover (alluvial fan) is about 5 m thickness with a velocity of 270 m/s. The rock below (Upper Cretaceous marly limestone) has a velocity of about 1400 m/s. Another noticeable increase of velocity is found at depth, between 70 and 100 m. The thickness of the cover and the rock characteristics are very variable below the town.
$V_{s,30}$ is 860 m/s and the site corresponds to ground type E in the Eurocode 8 (CEN, 2004) and SIA261 (SIA, 2014). The theoretical 1D SH transfer function computed from the inverted profiles shows deamplification at low frequency and a strong amplification at the resonance frequency of the cover around 13 Hz.

Acknowledgements

The authors thank Atefe Darzi and David Farsky for their help with the array measurements.

References

Burjánek, J., Gassner-Stamm, G., Poggi, V., Moore, J. R., and Fäh, D. (2010). Ambient vibration analysis of an unstable mountain slope. *Geophysical Journal International*, 180(2):820–828.

CEN (2004). *Eurocode 8: Design of structures for earthquake resistance - Part 1: General rules, seismic actions and rules for buildings*. European Committee for Standardization, en 1998-1: edition.

Edwards, B., Michel, C., Poggi, V., and Fäh, D. (2013). Determination of Site Amplification from Regional Seismicity : Application to the Swiss National Seismic Networks. *Seismological Research Letters*, 84(4).

Fäh, D., Kind, F., and Giardini, D. (2001). A theoretical investigation of average H/V ratios. *Geophysical Journal International*, 145(2):535–549.

Joyner, W. B., Warrick, R. E., and Fumal, T. E. (1981). The effect of Quaternary alluvium on strong ground motion in the Coyote Lake, California, earthquake of 1979. *Bulletin of the Seismological Society of America*, 71(4):1333–1349.

Poggi, V., Edwards, B., and Fäh, D. (2011). Derivation of a Reference Shear-Wave Velocity Model from Empirical Site Amplification. *Bulletin of the Seismological Society of America*, 101(1):258–274.

Poggi, V., Edwards, B., and Fäh, D. (2012a). Characterizing the Vertical-to-Horizontal Ratio of Ground Motion at Soft-Sediment Sites. *Bulletin of the Seismological Society of America*, 102(6):2741–2756.

Poggi, V. and Fäh, D. (2010). Estimating Rayleigh wave particle motion from three-component array analysis of ambient vibrations. *Geophysical Journal International*, 180(1):251–267.

Poggi, V., Fäh, D., Burjánek, J., and Giardini, D. (2012b). The use of Rayleigh-wave ellipticity for site-specific hazard assessment and microzonation: application to the city of Lucerne, Switzerland. *Geophysical Journal International*, 188(3):1154–1172.

Roesset, J. (1970). Fundamentals of soil amplification. In Hansen, R. J., editor, *Seismic Design for Nuclear Power Plants*, pages 183–244. M.I.T. Press, Cambridge, Mass.

SIA (2014). *SIA 261 Einwirkungen auf Tragwerke*. Société suisse des ingénieurs et des architectes, Zurich, Switzerland.

Wathelet, M. (2008). An improved neighborhood algorithm: Parameter conditions and dynamic scaling. *Geophysical Research Letters*, 35(9):1–5.